**Wind and Structures**, *Vol. 17, No. 5 (2013) 495-513*
DOI:http://dx.doi.org/10.12989/was.2013.17.5.495 

# Development and validation of a numerical model for steel roof cladding subject to static uplift loads

Amy C. Lovisa*[1], Vincent Z. Wang[1], David J. Henderson[2] and John D. Ginger[1]

[1]*School of Engineering and Physical Sciences, James Cook University, Townsville, Queensland 4811, Australia*
[2]*Cyclone Testing Station, James Cook University, Townsville, Queensland 4811, Australia*

*(Received August 10, 2012, Revised May 5, 2013, Accepted July 9, 2013)*

**Abstract.** Thin, high-strength steel roof cladding is widely used in residential and industrial low-rise buildings and is susceptible to failure during severe wind storms such as cyclones. Current cladding design is heavily reliant on experimental testing for the determination of roof cladding performance. Further study is necessary to evolve current design standards, and numerical modelling of roof cladding can provide an efficient and cost effective means of studying the response of cladding in great detail. This paper details the development of a numerical model that can simulate the static response of corrugated roof cladding. Finite element analysis (FEA) was utilised to determine the response of corrugated cladding subject to a static wind pressure, which included the anisotropic material properties and strain-hardening characteristics of the thin steel roof cladding. The model was then validated by comparing the numerical data with corresponding experimental test results. Based on this comparison, the model was found to successfully predict the fastener reaction, deflection and the characteristics in deformed shape of the cladding. The validated numerical model was then used to predict the response of the cladding subject to a design cyclone pressure trace, excluding fatigue effects, to demonstrate the potential of the model to investigate more complicated loading circumstances.

**Keywords:** finite element analysis; corrugated steel roof cladding; wind loading; testing; validation

## 1. Introduction

Steel roof cladding is commonly used as roofing in residential, industrial and commercial buildings throughout Australia. When subjected to extreme wind loads, such as those experienced in a cyclone, steel roof cladding can fail by either static pull-through or fatigue. Both mechanisms of failure can result in entire cladding sheets disengaging from their fasteners. The loss of cladding sheets, in the worst circumstances compromises the structural integrity of the building which can lead to total structural collapse (Walker 1975). In addition, dislodged sheets can become windborne debris, damaging neighbouring structures (Walker 1975, Walker *et al.* 1975).

Cyclone Althea caused wide-spread wind damage to roof cladding throughout Townsville in 1971. The magnitude and frequency of the wind damage to roof cladding prompted the revision of building regulations; suppliers of roof cladding were now required to test their roofing systems.

*Corresponding author, Ph.D. Research scholar, E-mail: amy.lovisa@jcu.edu.au


http://www.techno-press.org/?journal=was&subpage=8 ISSN: 1226-6116 (Print), 1598-6225 (Online)

These tests were based on the static pull-through strength of the cladding and were quickly implemented throughout Australia (Walker 1980). This included exchanging the customary thick and mild steel cladding to a thin, high-tensile steel alternative (Walker 2007). However, nearly all the improved cladding systems adopted in Darwin failed when Cyclone Tracy swept through in 1974 (Walker 1980). The damage investigations following Cyclone Tracy concluded that the widespread loss of roof cladding could be attributed to the fatigue of the roof cladding at its fixings (Beck 1975).

The improved static strength of the fastener systems and the change in cladding manufacture implemented following Cyclone Althea, resulted in the emergence of a new form of failure: cladding fatigue. The improved static strength enabled the cladding to undergo repeated loading during the cyclone which, in combination with the more brittle steel, generated fatigue cracks in the vicinity of a fastener. These cracks continued to propagate under repeated loading until a sizeable hole was present, thereby allowing the fastener head to pull through the cladding sheet. This phenomenon was recreated in experimental studies by Morgan and Beck (1977) soon after Cyclone Tracy, with the crack formations observed during the damage investigation closely resembling that created in the laboratory. Morgan and Beck (1977) also found that the fatigue strength of the cladding could potentially be as low as 15% of the static strength should the repeated load be applied a sufficient number of times.

In response to the devastation caused by Cyclone Tracy, and as a direct result of the research conducted by Morgan and Beck (1977), the first cladding fatigue test was implemented for cyclonic regions throughout Australia. The fatigue test, later known as the Darwin Area Building Manual (DABM) test, required the cladding system to undergo 10,000 cycles with a load range of 0 to 100% of the design load with a final overload cycle to 180% of the design load. The DABM test did not adequately simulate the cyclonic wind loads but was to some extent able to simulate the fatigue effects of these loads (Mahendran 1994a, 1995). The test provided an empirical means of determining the fatigue strength of the cladding, rather than the customary design equations stipulated by Australian Standards for other structural components.

In the following decades, extensive experimental research was conducted by Melbourne (1977), Beck and Stevens (1979), Mahendran (1989, 1990a,b, 1994a,b, 1995) and Xu (1993, 1995) to create a fatigue test that could simulate the fatigue effects of a cyclone along with the cyclonic wind loads themselves. The TR440 test was introduced nearly 15 years after Cyclone Tracy, and was adopted throughout Australia, excluding the Northern Territory (EBS 1978). The Northern Territory favoured the DABM test as it did not consider the TR440 to be an adequate alternative.

However, researchers were concerned that a number of cladding systems that passed the TR440 test were similar to those that had failed during Cyclone Tracy (Mahendran 1995). Consequently, the Low-High-Low (LHL) test developed by Mahendran (1994a, 1995) replaced the TR440 and DABM test. The LHL test was the first fatigue test to include the effect of both wind speed and direction of a cyclone. A modified version of Mahendran's (1994a, 1995) LHL test is employed in current testing and design standards.

The studies undertaken to understand the mechanism of cladding fatigue, and consequently develop a suitable fatigue test, were heavily reliant on experimental methods. The complexity of the cladding fatigue problem limited the availability of theoretical data. Previous studies created numerical models using finite element analysis (FEA) to supplement the lack of theoretical data. Mahendran (1990b, 1994b), Xu (1993), Xu and Teng (1994), Lucas *et al.* (1997a,b), and Mahaarachchi and Mahendran (2004, 2009a) have all developed various numerical models using FEA that could successfully predict the static response of roof cladding. The limitations of FEA

prevented the simulation of cladding fatigue and restricted the numerical models to the study of the static response of cladding. Nevertheless, studying the static response of cladding was invaluable as it identified the complex stress distributions surrounding the fasteners and the resulting plastic deformations. Fatigue cracks commonly originate in these regions of plastic deformation and Beck and Stevens (1979) found that cladding's fatigue response was directly related to the load at which cladding undergoes local plastic deformation.

The most recent numerical model of roof cladding was created by Mahaarachchi and Mahendran (2004, 2009a). This model was the first to incorporate the splitting characteristics of the steel cladding in the form of a stress-strain criterion (Mahaarachchi and Mahendran 2009b). It investigated the *static* response of the roof cladding for trapezoidal and rib-pan roof profiles and was particularly interested in simulating the static pull-through failure of the cladding. Mahaarachchi and Mahendran (2004, 2009a) used the validated numerical model of the cladding to perform a parametric study and the results were then used to create a design equation. Although the design equation was developed for the static pull-through failure of the cladding, Mahaarachchi and Mahendran (2004, 2009a) suggest that the equation could be applicable to cladding fatigue if a suitable reduction factor were applied. This was postulated based on the correlation between the static strength of the cladding and the fatigue strength of the cladding when subjected to *cyclic* loads, rather than *cyclonic* loads (Mahendran 1990a). This equation could potentially replace the costly fatigue tests currently stipulated by Australian Standards.

This paper presents the development and validation of a numerical model that can simulate the response of corrugated roof cladding subjected to static uplift pressure. The model incorporates the anisotropic material properties and the practical stress-strain relationship of a G550 corrugated cladding specimen with 0.42 mm base metal thickness (b.m.t.) as shown in Fig. 1. The corresponding values of the numerical study were compared with experimental results in order to validate the numerical model. The model predicted the characteristics in deformed shape, deflection, fastener reaction and – to an extent – the strain across the cladding. The numerical model described in this paper can predict the static pull-through failure of corrugated roof cladding and could potentially be evolved to model fatigue and subsequently fatigue failure.

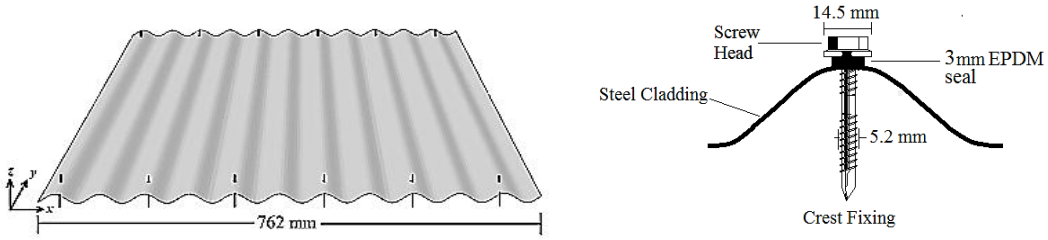


Fig. 1 Corrugated cladding sheet and crest fixing fastener (figure credited to Lovisa *et al.* (2012))

## 2. Experimental study

### *2.1 Experimental configurations*

In practice, steel roof cladding forms a continuous roof envelope. Cladding sheets are lapped

together at each longitudinal edge to seal the roof envelope and consequently prevent water from infiltrating the roof. The cladding is then fixed to timber or steel battens (purlins) beneath using fasteners that comprise a self-drilling screw and EPDM seal, as detailed in Fig. 1. The batten spacing can vary from 450 mm to 1800 mm, depending on the design wind load, creating a multi-span assembly. The battens are then connected in turn to the rafters or the top chord of a roof truss beneath. Fig. 2 details the various roofing components and connections that form the roof system.

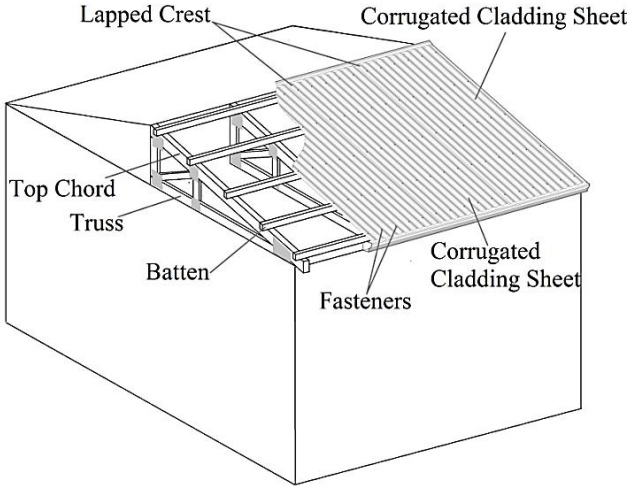


Fig. 2 Schematic of roof system

Due to the effects of flow separation, the cladding at the roof edge is subjected to the most severe wind loads with the first internal batten then experiencing the peak load (Morgan and Beck 1977, Beck and Stevens 1979). Flow separation at the roof edge creates conical vortices that apply significant negative pressures to the cladding beneath. These negative pressures are considered the limiting load that causes both static pull-through failure and fatigue failure. The turbulent nature of the wind flow around the building, coupled with the vortices in regions of flow separation, results in highly fluctuating wind loads (Holmes 2007).

For experimental testing, Beck and Stevens (1979) were able to effectively simulate the in situ behaviour of cladding using a double-span configuration, where the central support represents the critical first internal batten. Such a double-span assembly was utilized in both the experimental and numerical components of this investigation. A single cladding sheet with 900 mm spans was installed within an air box where it acted as the air box lid. Uniform uplift pressures were applied to the cladding sheet using a pressure load actuator (PLA). All experimental testing methods and apparatus used were consistent with that documented by Henderson (2010) and Henderson and Ginger (2011). In this investigation, the uplift pressures were steadily increased to various peak pressures and then decreased, similar to the general loading and unloading experienced by roof cladding during the passage of a cyclone. Four pressure sequences in total were applied sequentially to the cladding sheet where each sequence had the following peak pressures: 2 kPa, 3kPa, 5 kPa and 6 kPa. The purpose of the 2 kPa and 3 kPa pressure sequences was to investigate

the elastic response of the cladding. The 5 kPa and 6 kPa pressure sequences were consequently implemented to study the plastic response of the cladding, in particular the local plastic deformation of the cladding. For brevity only the loading of the cladding, and not the unloading, will be presented in this paper.

The experimental programme of this investigation was primarily used to provide data for validating the numerical model. Consequently, the three variables of interest were the deflection of the cladding, strain across the cladding and reaction at a fastener.

### *2.2 Materials and specimens*

The cladding under investigation was G550 corrugated, crest fixed cladding of 0.42 bmt as shown in Fig. 1. The rolling process when manufacturing the cladding sheets creates differing strengths and Young's moduli in the longitudinal and transverse directions. Table 1 gives the average properties of the coil from which the cladding originated and also highlights the variability of the material properties between coupon tests from a single coil (Rogers and Hancock 1997, Port Kembla Technical Services 2007). The complex shape of the cladding profile limits coupon testing from the sheet itself, so coupons cut from the coil prior to the roll forming of the cladding profile is considered an effective alternative and is common practice in industry.

All battens used to support the cladding were timber battens with a strength grade of MGP 12 or more (Standards Australia 2010). The cladding was fixed to the battens with fasteners comprising a screw and a neoprene seal that comply with AS 3566.2002 (Standards Australia, 2002). A timber batten was favoured over the commonly used steel top hat batten or the steel 'C' and 'Z' purlins to reduce the influence of the behaviour of the batten on the response of the cladding. Lucas *et al.* (1997a,b) explored the effects of the cladding-purlin connection using FEA. The models constructed by Lucas *et al.* (1997a,b) were primarily focused on studying the failure of cold-formed steel purlins under static wind uplift. Their model included the cladding sheet to more accurately simulate the nonlinear behaviour of the cladding-purlin system, as the cladding sheet provides rotational and shear stiffness to the purlin. Lucas *et al.* (1997a,b) found the behaviour of the purlins was strongly influenced by the behaviour of the cladding, and likely vice versa. Henderson (2010) experimentally investigated the influence of the purlin on the behaviour of the cladding and found the longitudinal movement of a fastener was enhanced by the rotation of the top flange of a purlin. Future models must subsequently include these effects to create a more accurate prediction of the response of roof cladding.

Table 1 Material Properties of cladding sheet (Port Kembla Technical Services 2007)

| Direction | Yield Stress (MPa) | | | Young's Modulus (GPa) | | |
|---|---|---|---|---|---|---|
| | *Average* | Maximum | Minimum | *Average* | Maximum | Minimum |
| Longitudinal | *785.4* | 799 | 774 | *219* | 237 | 207 |
| Transverse | *869.9* | 886 | 845 | *252* | 267 | 235 |

## 3. Development and validation of the finite element model

### *3.1 Model development*

The model developed for this investigation describes the entire double-span single-width cladding sheet, simulating the experimental conditions. Moreover, future application of the model includes an investigation into the effects of spatially varying pressure, necessitating the development of a computationally efficient model that describes an entire cladding sheet or a system of sheets. For this investigation, the lapped edges were not included in the model even though experimentally the bottom lap was used. The longitudinal edges were then modelled as free edges.

The cladding sheet in the numerical model was discretised using four-node, reduced-integration shell elements (S4R as in the commercial software package Abaqus) (Dassault Systems 2012). The S4R element is a general shell element developed to account for transverse shear deformation whilst being both accurate and computationally efficient for modelling geometrically nonlinear behaviour (Dassault Systems 2012).

The large model used in the numerical analysis required the selection of a mesh that reduced the simulation run time whilst avoiding considerably undermining the accuracy of the model. An element dimension of 5.8 mm was selected for discretising the model in the transverse ($x$) direction following a thorough visual inspection of the cladding profile. Studies by Xu (1995) found the fatigue performance of cladding, and presumably its response to a static load, were dependent on the profile, necessitating an accurate representation of the profile in the numerical model. An element size of 5.8 mm was considered to be the largest element dimension that maintained a sufficient representation of the cladding profile and any ensuing deformation.

A larger element dimension was used in the longitudinal ($y$) direction to reduce the requisite number of elements and subsequently the run time of the simulation. The selection of the element dimension was also limited by the allowable aspect ratio of the element. For this analysis, an aspect ratio of four was not exceeded to ensure accuracy of the results regardless of the versatility of the shell elements (Potts and Zdravkovic 2001).

In regions surrounding the fasteners, a finer mesh was used to accommodate the large expected variations in the elastic and plastic strains. Elements with an aspect ratio of one, resulting in an element size of 5.8 mm x 5.8 mm, were used to help maintain the accuracy within the region. The element size was then reduced further to 1-2 mm in the areas immediately surrounding the edge of the fastener hole to improve convergence issues associated with the large plastic strain and local plastic deformation experienced by the region. A mesh sensitivity study was used to determine the optimum element sizes for the finer mesh. The study focused on the effects of the element size with respect to the convergence of the solution. Fig. 3 describes the discretised numerical model, showing the various element sizes in each region.

The numerical model accounted for the anisotropic and nonlinear material properties of the cladding, as previously described in Table 1. The strength through the cladding profile ($z$ direction) was assumed to be equal in strength to the weaker direction, and Poisson's ratio was taken as 0.3 for all directions. The material properties of the cladding sheet, including the strain-hardening characteristics, were incorporated into the numerical model in terms of a true stress-plastic strain curve. This stress-strain curve provided a reference for describing the strengths in each direction of the material, and was included in the model in tabular form. The strengths in each direction were then defined in terms of a ratio to the reference stress-strain curve, where the stress-strain curve was scaled so that the yield stress and Young's modulus of the curve was equivalent to those

shown in Table 1. The true stress-plastic strain curve for the transverse direction was used as the reference stress-strain curve in the model. Both the nominal and the reference stress-strain curves for the transverse direction are shown in Fig. 4, which emphasises the strain-hardening characteristics of the material. It was also assumed that the material possessed isotropic hardening qualities as only positive pressure were applied.

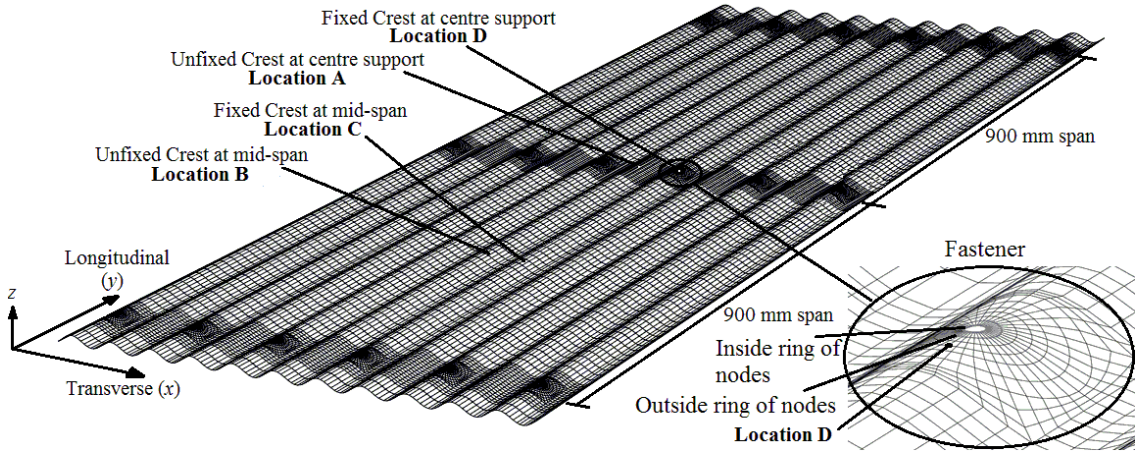


Fig. 3 Numerical model mesh

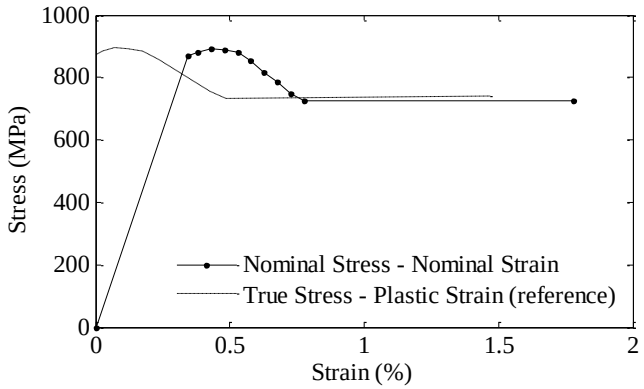


Fig. 4 Stress-Strain curves for the transverse direction

The boundary conditions of the numerical model were derived from the fasteners fixing the cladding to the battens. Each fastener was simplified as two rings of partially restrained nodes, one ring along the inside edge of the fastener hole and a second ring of nodes placed 4 mm outside the hole edge where the outer edge of the neoprene seal would, in practice, be located. The nodes constituting the innermost ring were fixed from translating but were free to rotate about all axes, simulating the ability of the cladding to rotate beneath the neoprene seal. In practice, the neoprene

seal disperses the fastener reaction over a small area of the cladding, influencing the load at which the cladding buckles and the formation of the localized deformation. Subsequently, the second ring of nodes was included to simulate this dispersal effect where the nodes were fixed from translating vertically (in the *z* direction) while free to rotate. An additional limitation of using fixed nodes to simplify the support was the inability of the model to account for the hyperelasticity of the seal (Mahaarachchi and Mahendran 2004). Fig. 3 shows the two-ring configuration of the restrained nodes.

The numerical model utilized a uniform surface follower load to simulate the static uplift pressure. The loads were incorporated into a general step analysis in Abaqus to ensure any deformation accumulated as the loading sequence progressed (Dassault Systems 2012). The loading sequences applied in the numerical model duplicated the experimental pressure sequences.

Two analysis types were used, a nonlinear static analysis and a nonlinear dynamic analysis. A nonlinear static analysis was implemented to model the response of the cladding prior to buckling which successfully reduced the total run time of the simulation. However, the static analysis could not simulate the buckling and post buckling behaviour of the cladding, necessitating the implementation of a nonlinear dynamic analysis. A nonlinear dynamic analysis can simulate the transformation of excess strain energy into kinetic energy which occurs during buckling. Consequently, the dynamic analysis was the preferred method for modelling buckling as it ensured a more accurate prediction of the change in strain surrounding the fasteners. The nonlinearity of the analyses accounted for the geometric nonlinearity of the cladding, such as the large deflections and local buckling.

The excessive run time was further reduced by using an implicit form of the dynamic analysis. An implicit dynamic analysis uses larger and fewer increments than the explicit analysis and consequently is more suited to models with a longer loading sequence where the loading changes more slowly.

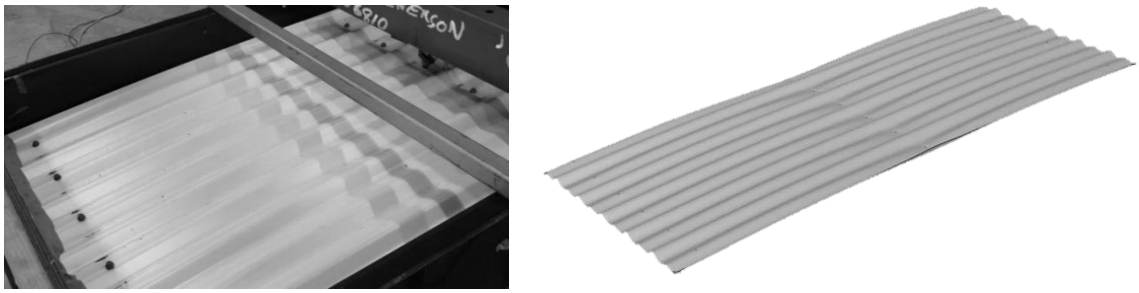

(a) (b)

Fig. 5 Buckling of Cladding sheet in (a) experiment and (b) numerical model

### *3.2 Model validation*

The accuracy of the numerical model was validated through a comparison of the numerical results with the corresponding experimental results. In addition, a visual inspection of the deformed shape was included to further assess the ability of the model to simulate the response of the cladding. The numerical model successfully simulated the local dimpling of the fastened crests

prior to buckling, the complex cross-sectional distortion characteristic of buckling and the permanent deformation of the crests following unloading of the cladding sheet. Fig. 5 demonstrates the capability of the model to predict the complex cross-sectional distortion characteristic of local plastic collapse as it emphasises the consistencies between the deformed shape observed in the experiment and the deformed shape of the model at the equivalent load. The numerical model also successfully simulated the permanent deformation following unloading of the cladding sheet, as shown in Fig. 6. The model captured the bulges in the rise of the crests which were difficult to discern visually but obvious to the touch during the experiment. For clarity, Fig. 6(b) shows Location D cut along the transverse direction and contoured with respect to vertical ($z$) deflection.

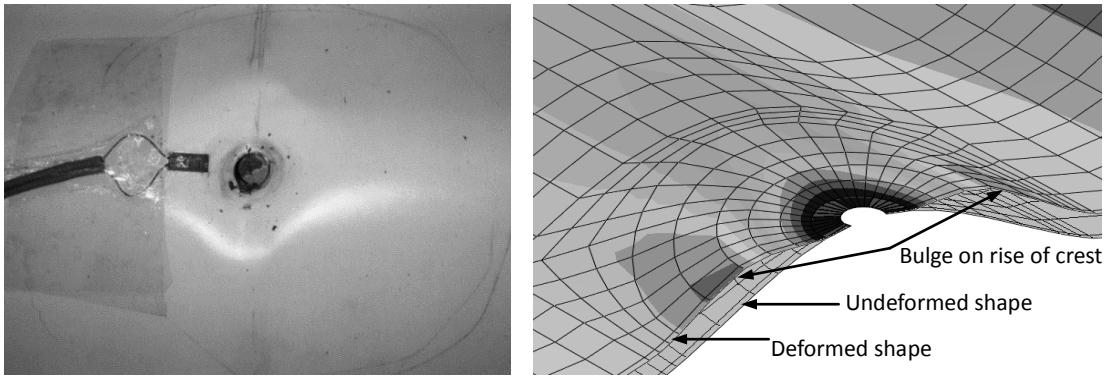


Fig. 6 Permanent local dimpling of fastened crest in (a) experiment and (b) numerical model

Following visual inspection of the deformed shape of the numerical model, the experimental and numerical deflections, strain and fastener reaction were compared to assess the ability of the model to predict the response of the cladding. The numerical results are presented in terms of an envelope of potential values to provide a more comprehensive comparison of the results. This envelope of values was developed using the minimum, maximum and average material properties of the coil from which the cladding sheet originated which are provided in Table 1.

The ability of the model to predict the upward deflection of the cladding was assessed by comparing the deflection at three separate locations on the cladding sheet; specifically location A, B and C as identified in Fig. 3. All three deflections were compared with the corresponding experimental results from all four pressure sequences. The comparison for the elastic (3 kPa) and plastic (5 kPa, 6 kPa) pressure sequences are shown graphically in Figs. 7, 8 and 9 respectively.

The results for the 2 kPa pressure sequence closely resembled the results from the 3 kPa pressure sequence and were subsequently not included in this paper. Figs. 7, 8 and 9, show good agreement between the numerical and experimental results for the deflection at all recorded locations. The numerical model predicted a nonlinear relationship between load and deflection within the defined elastic deformation stage (where the applied load is less than 3 kPa) which was first observed experimentally. Fig. 9 also demonstrates the ability of the model to predict the local plastic collapse of the cladding, and the resulting geometric stiffening.

Fig. 9 clearly shows that buckling of the cladding occurred experimentally at an applied

pressure of 4.8 kPa during the 6 kPa pressure sequence. However, the 5 kPa pressure sequence did not have a distinguishable buckling stage like that clearly described in the 6 kPa pressure sequence.

During the 5 kPa pressure sequence there was some visible yielding surrounding the fasteners along the centre support, although local plastic collapse was not observed. This yielding would result in some residual plastic strain following unloading of the cladding sheet. The remaining plastic strain would likely have reduced the load required to cause buckling in the 6 kPa pressure sequence, which is why buckling then occurred at an applied pressure less than 5 kPa. Both the results from the 5 kPa and 6 kPa pressure sequence are consistent with those documented by Mahendran (1994b) and Xu and Reardon (1993) who found buckling to occur at an applied pressure of around 5 kPa for the equivalent test spans. The numerical results are also consistent with the experimental results, with the model predicting that buckling would occur at an applied pressure of 4.7 kPa to 5.0 kPa depending on the material properties of the sheet. A comparison of the experimental and numerical results for the applied pressure at buckling is presented in Table 2.

Other variations in the experimental results can also be observed, for example the difference between the numerical and experimental results appears greater for the 6 kPa pressure sequence than that of the 3 kPa pressure sequence. This variation can be attributed to a number of experimental factors, such as some small movement of the supporting structure, settlement of the screw heads and seals, and residual permanent deformation and stress from the previous pressure sequence. Numerical factors could also be attributing to the larger variation between numerical and experimental results. For example, the simplification of the fastener as two rings of partially restrained nodes would limit the predicted deflection as the additional deflection caused by the compression of the seal is not included in the model. Under large uplift loads the seal would compress and potentially allow up to an additional 2 mm in uplift, this likely being the cause of the model under-predicting the deflection for the 6 kPa pressure sequence. The effects of excluding the neoprene seal were less pronounced in the 3kPa pressure sequence given that the seal was only slightly compressed at an applied pressure of 3 kPa.

Fig. 9 also illustrates the effects of varying the material properties on the upward deflection of the cladding. The change in yield stresses and Young's moduli investigated here had minimal effect on the magnitude of the upward deflection, but did result in different loads at which buckling occurred. The material properties also affected the mode of buckling with the models that used the maximum and average material properties, exhibiting a two-stage buckling process. The model that used the minimum material properties exhibited only a single stage buckling process, similar to that described experimentally. A visual inspection of the deformed shape shows a sudden dimpling of the crests at the first stage of buckling, followed by a complete flattening of the fastened crests for the second stage. Experimentally, these two stages were also observed, although stage two immediately followed stage one without delay. The delay between the two stages for the models that used the maximum and average material properties can be attributed to the different strain-hardening characteristics of the material properties. The stress-strain curve used to define the maximum material properties possessed the most significant strain-hardening component whilst the stress-strain curve used to define the minimum material properties had a negligible strain hardening component. The magnitude of the delay between stages reflects the magnitude of the strain-hardening included in each respective model.

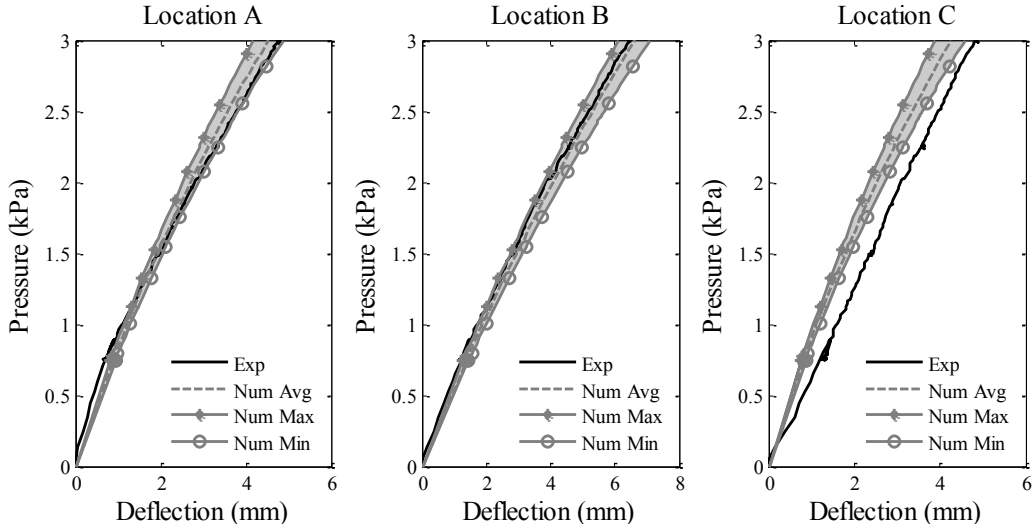


Fig. 7 Load-deflection curves for a peak pressure of 3 kPa (elastic response)

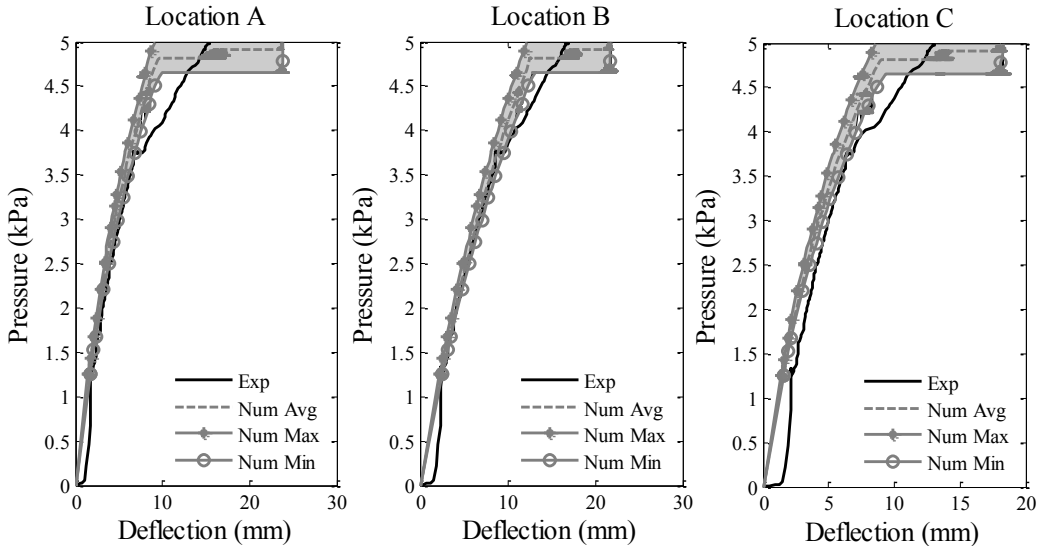


Fig. 8 Load-deflection curves for a peak pressure of 5 kPa (plastic response)

The ability of the model to predict the strain across the cladding was also assessed. The global and local response of the cladding was of interest so a comparison of the strain at both the mid-span and centre support was required. The longitudinal strain at locations A, B, C and D (as identified in Fig. 3) was recorded experimentally to provide an adequate comparison with the numerical results. The strain on the top surface of the cladding was measured at locations A and D while both the top and bottom surface strain was recorded at the mid-span locations (B and C); hereby referred to as Ba and Ca for the bottom strain, and Bb and Cb for the top strain. For the model validation the experimental and numerical results were compared in terms of strain as a

single strain gauge in the longitudinal direction was employed at each location. The constitutive description of the model includes anisotropic elasticity for a triaxial stress state and any stress predictions made by the model accounts for the significant transverse stress in the cladding sheet.

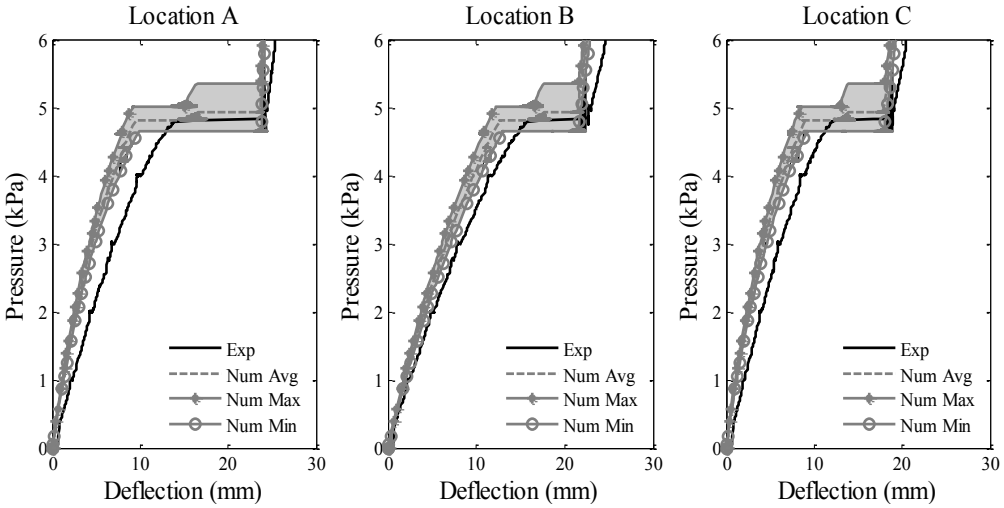


Fig. 9 Load-deflection curves for a peak pressure of 6 kPa (plastic response)

Table 2 Applied pressure at buckling

| | | Applied Pressure (kPa) | Experimental/Numerical |
|---|---|---|---|
| *Experimental* | | *4.82* | - |
| Numerical | Average | 4.83 | 1.00 |
| | Max | 5.02 | 0.96 |
| | Min | 4.65 | 1.04 |

Figs. 10, 11 and 12 present the longitudinal strains obtained numerically and experimentally for the 3kPa, 5 kPa and 6 kPa pressure sequences respectively. The strain results for the 2 kPa pressure sequences are similar to the results from the 3 kPa pressure sequence. Only the numerical results from the model that used the average material properties have been included in Figs. 10, 11 and 12 as the different material properties also produced only very small variations in the strain.

Figs. 10, 11 and 12 show very good agreement between the numerical and experimental results for the longitudinal strain at locations A and C. The model successfully predicted the strain on both the top and bottom surface of the cladding sheet for location C and effectively described the difference between the top and bottom surface strains for location B. Fig. 12 demonstrates the ability of the model to capture the overall behaviour of the strain across the cladding for the plastic response, including the sudden decrease and increase in magnitude respectively caused by buckling. These sudden changes in strain are likely generated by the large upward deflections in the cladding sheet, in conjunction with a large tensile membrane stress. The varying magnitudes of the change in strain for each location could be attributed to a counteracting or contributing (depending on the location) bending stress. For all load sequences the model consistently

maintained a better prediction for the strain at locations A and C; in regions that are the most restrained by fasteners.

The model appears to be limited in predicting the strain at locations B and D. The variation between the experimental and numerical results is likely due to a combination of experimental and numerical factors, some of which were mentioned earlier with reference to deflection. In particular, the discrepancy between the numerical and experimental results for the strain adjacent to a fastener (location D) is possibly due to the simplification of the fastener as two rings of partially restrained nodes. Although the simplified boundary conditions of the model limit the prediction of strain surrounding a fastener, the resulting reduction in simulation run time is significant.

For the 6 kPa pressure sequence, only the numerical and experimental strain at three of the four locations could be compared. The strain gauge adjacent to the fastener at the centre support (location D) did not provide usable data after the area yielded during the 5 kPa pressure sequence. Fig. 11 shows the strain results for the gauge in question and identifies the point at which the limits of the gauge were exceeded (an applied pressure of 3.8 kPa). The difficulty of recording the strain in regions of high plasticity warranted the need for recording the fastener reaction and strains at the mid-span, all of which provide usable data for both the elastic and plastic response.

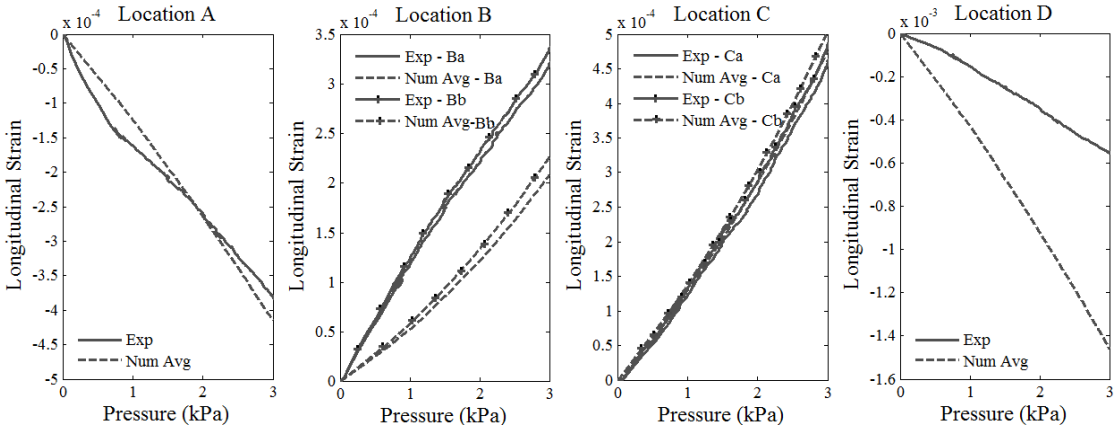


Fig. 10 Strain-load curves for 3 kPa pressure sequence

The numerical model successfully predicted the fastener reaction for all pressure sequences, with Fig. 13 showing good agreement between experimental and numerical data. The model successfully predicted the reduction in fastener reaction caused by buckling which has been documented by Xu and Reardon (1993) and is present in the experimental fastener reaction-load curve shown in Fig. 13. The fastener reaction is particularly important as the fastener load governs when local plastic deformation occurs, irrespective of the span of the cladding (Mahendran 1990a). Mahendran (1990a) and Xu and Reardon (1993) found buckling to occur at a fastener reaction of approximately 650 N which is consistent with both the experimental and numerical results. Table 3 details the experimental and numerical fastener reaction at buckling and compares them in terms of a ratio of experimental to numerical results.

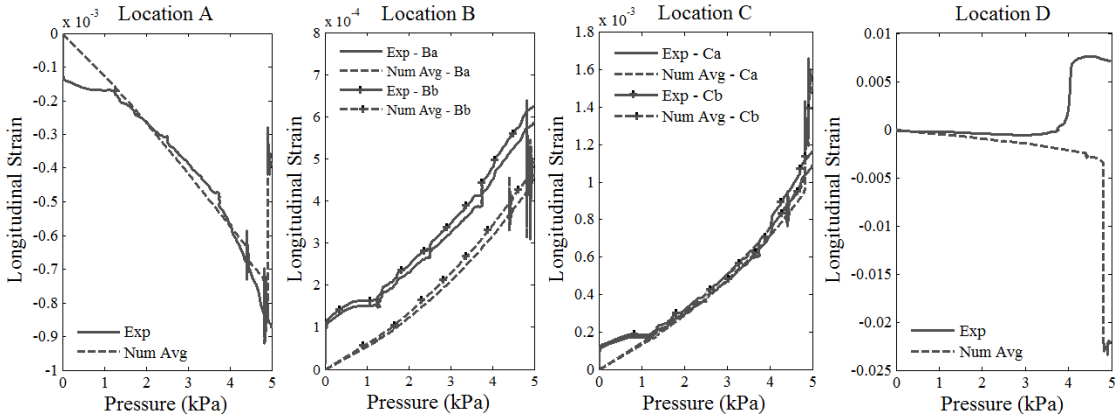


Fig. 11 Strain-load curves for 5 kPa pressure sequence

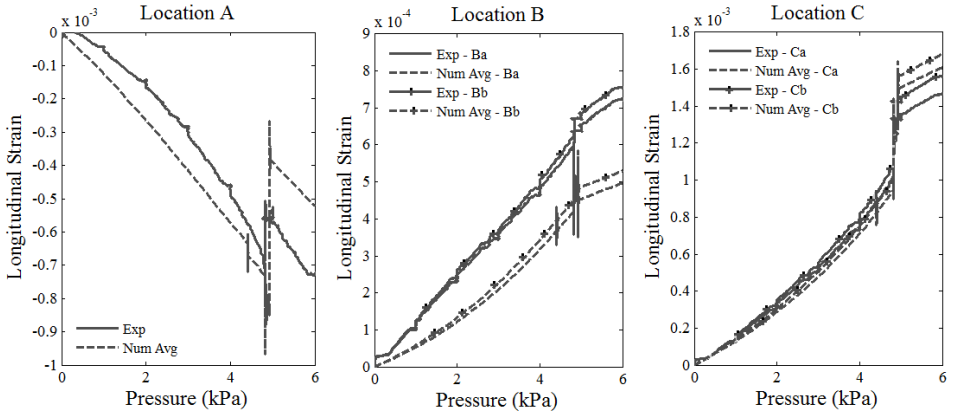


Fig. 12 Strain-load curves for 6 kPa pressure sequence

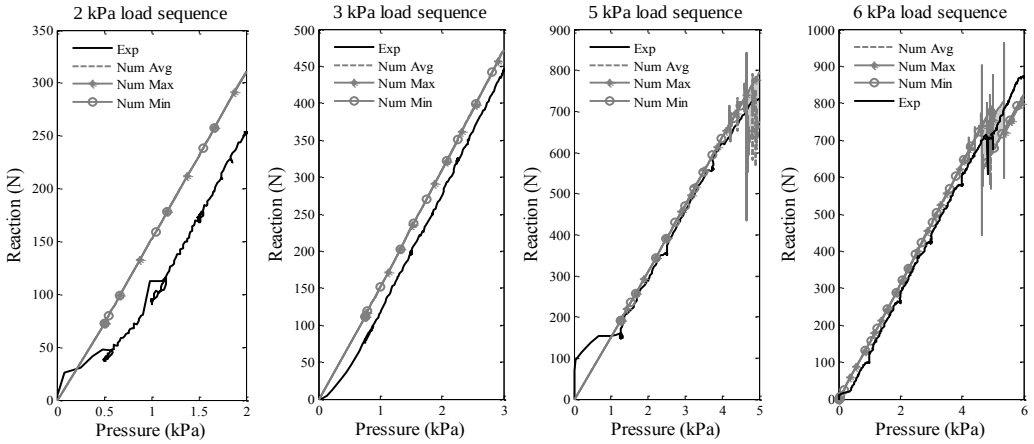


Fig. 13 Fastener reaction-load curves for all pressure sequences

Table 3 Fastener reaction at buckling

| | | Fastener Reaction (N) | Experimental/Numerical |
|---|---|---|---|
| *Experimental* | | *681* | - |
| | Average | 724 | 0.94 |
| Numerical | Max | 763 | 0.89 |
| | Min | 714 | 0.95 |

## 4. Response prediction based on the validated numerical model

A major benefit of the validated numerical model is the ability to explore the effects of loading on a cladding sheet in greater detail than is experimentally feasible. This includes the ability to monitor the development of the stress within the entire cladding sheet at each stage of loading. Fig. 14 presents a von Mises stress contour on the deformed shape of the cladding sheet at an applied pressure of 4.4 kPa. At this point in the pressure trace the fastened crests at the central supports have begun to dimple. The stress contour suggests that the first internal fastened crest experienced the largest magnitude of stress. These high stresses are responsible for the fatigue cracking that commonly originates at the first internal crest, as documented by both Mahendran (1989) and Henderson (2010). Fig. 14 also shows the larger deflection of the unfixed crest between the fastened crest at the edge and the first internal fastened crest which was also observed experimentally by Henderson (2010).

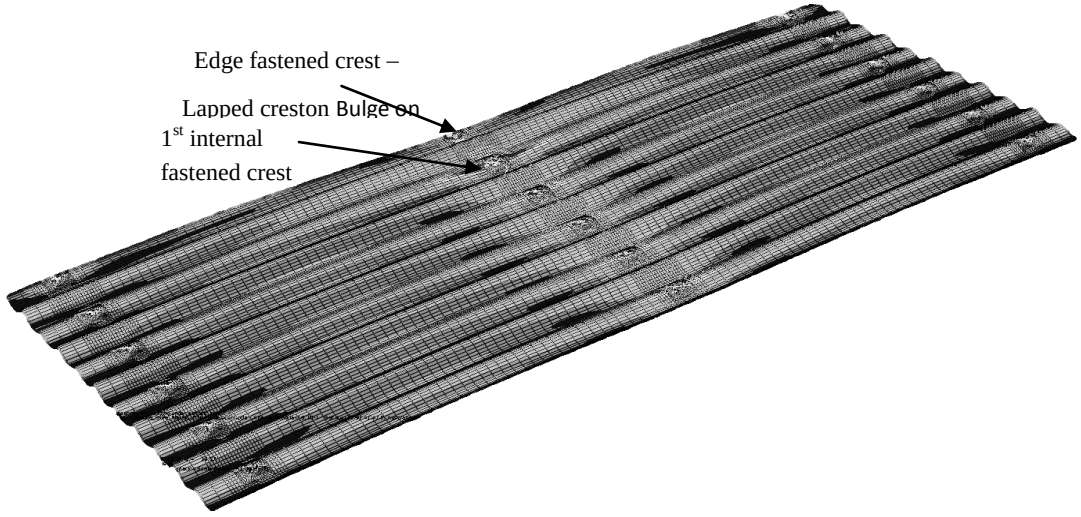


Fig. 14 Von Mises stress contour under 4.4 kPa of pressure

An additional benefit of the numerical model is its ability to simulate unique and complex loading sequences. A one minute sample of a design cyclone pressure trace was selected and input into the numerical model. The design cyclone pressure trace used in the analysis was developed by

Henderson *et al.* (2009) based on the design cyclone created by Jancauskas *et al.* (1994) and using data provided by the United States' National Institute of Standards and Technology (NIST). The pressure trace accounted for the passage of the cyclone and included the resulting change in wind speed and direction. However, the sample used as input in the numerical model primarily contained pressures within the elastic deformation stage. Only the last ten seconds of the sample contained pressures that exceeded the buckling load of the cladding.

Figs. 15(b) and 15(c) present the deflection and stresses within the cladding subject to a one minute sample of the design cyclone pressure trace shown in Fig. 15(a). Given the inability of the model to simulate the cracking at a fastener, the results presented in Fig. 15 are only relevant to an uncracked cladding specimen. The input of the design cyclone pressure trace was primarily to exercise the ability of the model to apply complex pressure sequences. The results shown in Fig. 15 are also consistent with the behaviour of the cladding observed during the experiments.

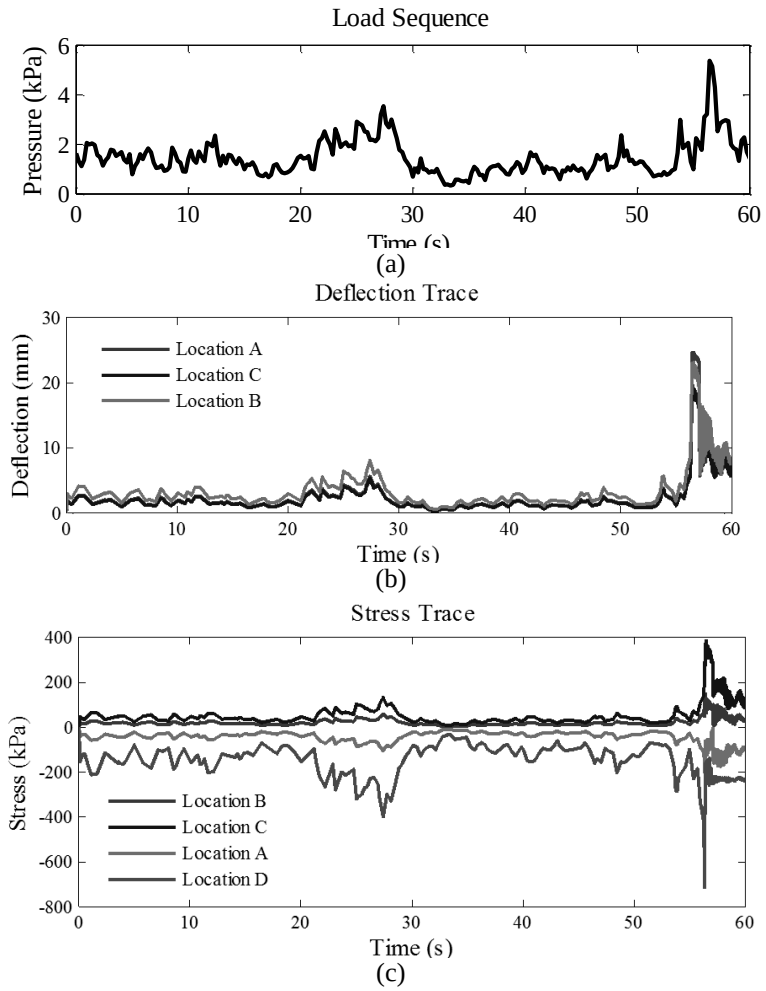


Fig. 15 Cyclone trace (a) and the resulting numerical displacement (b) and stress (c) traces

## 5. Conclusions

The response of corrugated steel roof cladding subject to a static uplift pressure was investigated both experimentally and numerically. Using finite element analysis, a numerical model that replicated the experimental conditions was developed. The numerical model incorporated the anisotropic material properties of the cladding, including the strain-hardening characteristics, and was able to predict the deformed shape of the cladding, the deflection of the cladding and the fastener reaction. The model appeared to be less capable of predicting the strain across the cladding with an accurate prediction of strain at two of the four recorded locations. A combination of numerical and experimental factors are likely attributing the variation between experimental and numerical results.

The numerical model also identified the effects of varying the material properties of the cladding sheet. For this investigation, the yield stress in the longitudinal direction was varied by at least 25 MPa and the Young's Moduli of the cladding was varied by 30 GPa. These small variations in material properties did not significantly affect the magnitude of the deflection or strain, but did change the load at which buckling occurred and the mode of buckling itself.

A validated numerical model, such as the one presented in this paper, provides a cost effective and efficient means of studying the response of cladding. Extensive studies using such a numerical model would provide a greater understanding of the mechanism of roof cladding failure during cyclones and subsequently improve current roof cladding design. Current design standards require costly and time consuming experimental methods to assess the performance of steel roof cladding. Further investigation into the mechanism of cladding failure could potentially lead to a design equation that minimises dependence on empirical relationships.

## References

Beck, V. (1975), *Appraisal of roof cladding under dynamic wind loading – Cyclone Tracy Darwin 1974: Appendix 4*, Report on Cyclone Tracy – Effect on buildings – Dec 1974, (Ed. G. Walker), Australian Department of Housing and Construction.

Beck, V. and Stevens, L. (1979), "Wind loading failures of corrugated roof cladding", *Civil Eng. Transactions, IE Australia*, **21(**1), 45-46.

Dassault Systems (2012), *Abaqus example problems manual*, Dassault Systems Simulia Corp, USA.

Experimental Building Station (EBS) (1978), *TR440 - Guidelines for the testing and evaluation of products for cyclone prone areas*, Sydney, Australia.

Henderson, D.J. (2010), *Response of pierced fixed metal roof cladding to fluctuating wind loads*, *Ph.D. Thesis*. Townsville (Australia), James Cook University.

Henderson, D.J. and Ginger J.D. (2005), "Fatigue failure of roof components subjected to wind loading", *Proceedings of the Australian Structural Engineering Conference*, Newcastle (Australia), September.

Henderson, D.J. and Ginger J.D. (2011), "Response of pierced fixed corrugated steel roofing systems subjected to wind loads", *Eng. Struct.*, **33**(12), 3290-3298.

Henderson, D.J., Ginger J.D. and Morrison M. (2009), "Simulated tropical cyclonic winds for low cycle fatigue loading of steel rofing", *Wind Struct.*, **12**(4), 383-400.

Holmes, J.D. (2007), *Wind loading of structures*, 2nd Ed., Taylor and Francis, New York.

Jancauskas, E.D., Mahendran, M. and Walker, G.R. (1994), "Computer simulation of the fatigue behaviour of roof cladding during the passage of a tropical cyclone", *J. Wind Eng. Ind. Aerod*., **51**(2), 215-227.

Leicester, R.H. and Reardon, G.F. (1976), *Wind damage in Australia: A pictorial review with particular reference to domestic and other low rise structures.* CSIRO Division of Building Research, Victoria

(Australia).
Lovisa, A.C., Wang, V.Z., Henderson, D.J. and Ginger, J.D. (2012), "A finite element model for pierced-fixed, corrugated metal roof cladding subject to uplift wind loads", *Proceedings of the Australasian Structural Engineering Conference*, Perth, Australia, July.
Lucas, R.M., Al-Bermani, F.G.A. and Kitipornchai, S. (1997a), "Modelling of cold-formed purlin-sheeting systems - Part 1: full model", *Thin Wall. Struct.*, **27**(3), 223-243
Lucas, R.M., Al-Bermani, F.G.A. and Kitipornchai, S. (1997b), "Modelling of cold-formed purlin-sheeting systems - Part 2. simplified model", *Thin Wall. Struct.*, **27**(4), 263-286
Mahaarachchi, D. and Mahendran, M. (2004), "Finite element analysis and design of crest-fixed trapezoidal steel claddings with wide pans subject to pull-through failures", *Eng. Struct.*, **26**(11), 1547-1559.
Mahaarachchi, D. and Mahendran, M. (2009a), "Wind Uplift Strength of trapezoidal steel cladding with closely spaced ribs", *J. Wind Eng. Ind. Aerod.*, **97**(3-4), 140-150.
Mahaarachchi, D. and Mahendran, M. (2009b), "A strain criterion for pull-through failures in crest-fixed steel claddings", *Eng. Struct.*, **31**(2), 498-506.
Mahendran, M. (1989), *Fatigue behaviour of corrugated rooding under cyclic wind loading*, Cyclone testing station technical report 35, James Cook University, Townsville (Australia).
Mahendran, M. (1990a), "Fatigue behaviour of corrugated roofing under cyclic wind loading", *Civil Eng. Transactions, IE Australia*, **32**(4), 219-226.
Mahendran, M. (1990b), "Static behaviour of corrugated roofing under simulated wind loading", *Civil Eng. Transactions, IE Australia*, **32**(4), 211-218.
Mahendran, M. (1994a), "Steel roof claddings under simulated cyclonic wind forces", *Civil Eng. Transactions, I.E. Australia*, **36**(1), 1-9.
Mahendran, M. (1994b), "Behaviour and design of crest-fixed profiled steel roof claddings under wind uplift", *Eng. Struct.*, **16**(5), 368-376.
Mahendran, M. (1995), "Appropriate fatigue loading sequence for roof claddings", *Eng. Struct.*, **17**(7), 476-484.
Melbourne, W.H. (1977), "Loading cycles for simulation of wind loading", *Proceedings of the Workshop on Guidelines for Cyclone Product Resting and Evalutation*, Experimental Building Station, Department of Construction, Sydney, July.
Morgan, J.W. and Beck, V.R. (1977), "Failure of sheet-metal roofing under repeated wind loading", *Civil Eng. Transactions, I.E. Australia*, **19**(1), 1-5.
Port Kembla Technical Services (2007), *Tensile testing result summary*, Bluescope Steel, Port Kembla (Australia).
Potts, D. and Zdravkovic, L. (2001), *Finite element analysis in geotechnical engineering: application*, Thomas Telford, London.
Rogers, C.A. and Hancock, G.J. (1997), "Ductility of G550 sheet steels in tension", *J. Struct. Eng. - ASCE*, **123**(12), 1586-1594.
Standards Australia (2002), *Self drilling screws for the building and construction industries*, Australian Standard AS3566-2002, Standards Australia, Sydney, New South Wales (Australia).
Standards Australia (2010), *AS1720.1-2010: timber structures - design methods*, Australian Standard AS1720.1-2010, Standards Australia, Sydney, New South Wales (Australia).
Walker, G. (1975), *Report on cyclone tracy - effects on buildings - Dec 1974*, Australian Department of Housing and Construction, Melbourne (Australia).
Walker, G.R. (1980), "A review of the impact of Cyclone Tracy on Australian building regulations and practice", *Civil Eng. Transactions, I.E. Australia*, **22**(2), 100-107.
Walker, G.R. (2007), *The birth of the cyclone testing station – personal recollections*, Prepared as a Contribution to the 30th Anniversary Celebrations of the Founding of the Station in November 1977, James Cook University.
Walker, G.R., Minor, J.E. and Marshall, R.D. (1975), "The Darwin Cyclone - valuable lessons in structural design", *Civil Eng. - ASCE*, **45**(12), 82-86.

Xu, Y.L. (1993), *Wind-induced fatigue loading on roof cladding of low-rise buildings*, Cyclone testing station technical report 41, James Cook University, Townsville (Australia).
Xu, Y.L. (1995), "Fatigue performance of screw-fastened light-guage-steel roofing sheets", *J. Struct. Eng. - ASCE*, **121**(3), 389-398.
Xu, Y.L. and Reardon, G.F. (1993), "Test of screw fastened profiled roofing sheets subject to simulated wind uplift", *Eng. Struct.*, **15**(6), 423-430.
Xu, Y.L. and Teng, J.D. (1994), "Local plastic failure of light gauge steel roofing sheets: finite element analysis versus experiment", *J. Constr. Steel Res.*, **30**(2), 125-150.

*JH*